Improving stability of stabilized and multiscale formulations in flow simulations at small time steps

M.-C. Hsu [a,1], Y. Bazilevs [a,2], V.M. Calo [b,c,2], T.E. Tezduyar [d,3], and T.J.R. Hughes [e,4]

[a]*Department of Structural Engineering, University of California, San Diego, 9500 Gilman Drive, Mail Code 0085, La Jolla, CA 92093, USA*

[b]*Earth and Environmental Science and Engineering, King Abdullah University of Science and Technology, P.O. Box 55455, Jeddah 21534, Saudi Arabia*

[c]*Applied Mathematics and Computational Science, King Abdullah University of Science and Technology, P.O. Box 55455, Jeddah 21534, Saudi Arabia*

[d]*Mechanical Engineering, Rice University - MS 321, 6100 Main Street, Houston, TX 77005, USA*

[e]*Institute for Computational Engineering and Sciences, The University of Texas at Austin, 201 East 24th Street, 1 University Station C0200, Austin, TX 78712, USA*

Abstract

The objective of this paper is to show that use of the element-vector-based definition of stabilization parameters, introduced in [1, 2], circumvents the well-known instability associated with conventional stabilized formulations at small-time-steps. We describe formulations for linear advection-diffusion and incompressible Navier-Stokes equations and test them on three benchmark problems: advection of an L-shaped discontinuity, laminar flow in a square domain at low Reynolds number, and turbulent channel flow at friction-velocity Reynolds number of 395.

Key words: variational multiscale methods, stabilized methods, advection-diffusion equation, element-vector-based τ, incompressible Navier-Stokes equations, turbulence modeling, turbulent channel flow

[1] Graduate Research Assistant
[2] Assistant Professor
[3] James F. Barbour Professor of Mechanical Engineering and Materials Sciences
[4] Professor of Aerospace Engineering and Engineering Mechanics, Computational and Applied Mathematics Chair III

1 Introduction

Residual-based variational multiscale methods were recently advocated and successfully used for turbulence modeling in the LES regime in [3]. The main idea of the variational multiscale approach is the a-priori decomposition of the underlying functional weighting and solution spaces into coarse and fine scales. The coarse scales are associated with the numerical approximation, while the fine scales are associated with the subgrid scales and, as a result, require modeling. Residual-based models were proposed in [3], where the fine-scale field was assumed to be proportional to the residuals of the coarse scale. The proportionality factors, the so-called τ's, are obtained through asymptotic scaling arguments that were developed in stabilized methods theory over the last three decades (see, e.g., [1, 4–12]). Recently τ's were identified with low-order moments of the fine-scale Green's function, a fundamental object in the design and analysis of variational multiscale methods (see [13]).

Stabilization parameters play a critical role in the success of the stabilized and variational multiscale methodologies. Despite decades of research devoted to them, several outstanding issues remain. One such issue, that to this day generates much debate in the community, is the dependence of τ's on the time step for time-dependent simulations. In particular, conventional definitions of τ's that include the time-step are not well-behaved for small time steps in both time-dependent and steady-state regimes. On the contrary, conventional definitions of τ's that do not include the time-step size are not sufficiently robust for complex flow situations. Evidence of the latter fact will be shown in the numerical example portion of this paper.

In recent works, Harari [14] and Harari and Hauke [15] examined the small-time-step problem in the context of diffusion and advection-diffusion problems, respectively, and introduced simple modifications to τ's to account for the small-time-step limit.

The small-time-step deficiency was also addressed in Codina *et al.* [16] in the context of variational multiscale methods for incompressible flow by means of so-called "dynamic subgrid scales." In [16] an ordinary differential equation and asymptotic scaling arguments are used to advance the fine-scale field in time. The fine-scale field becomes a "history variable" that needs to be stored at each integration point, leading to a computational structure that is similar to that for inelastic constitutive equations in computational solid mechanics (see, e.g., Simo and Hughes [17]). Calculations and an analytical stability analysis confirm the good behavior of the dynamic subgrid scales approach [16]. A simplified implementation that only requires an additional vector of the size of the global unknowns may be found in the recent article by Houzeaux and Principe [18].

In this article, we present another approach that is based on the element-vector-based (EVB) definition of τ's proposed in [1, 2]. In this methodology, τ's are built by examining relative magnitudes of the terms appearing in the variational equations, which is yet another form of a scaling argument. Our calculations confirm that this methodology is robust for all time-step sizes. Furthermore, an appropriate definition of the stabilization parameter for the steady flow regime is recovered.

In Section 2 we present the continuous and discrete versions of the variational formulation of the linear time-dependent advection-diffusion equation, show the details of the formulation of the conventional and EVB stabilization parameters, and compare their performance on the benchmark example of advection of an L-shaped discontinuity. In Section 3 we present the residual-based variational multiscale formulation of the incompressible Navier-Stokes equations and compare the performance of the conventional and EVB stabilization parameters on two benchmark problems: laminar flow in a square domain at low Reynolds number and turbulent channel flow at friction-velocity Reynolds number of 395.

In all numerical calculations we use the generalized-α method for time integration with the high frequency damping parameter ρ_∞ set to 0.5 (see, e.g., [19, 20]). We use B-splines of maximal continuity for the spatial discretization as we have demonstrated these provide superior accuracy and robustness compared with C^0-continuous finite elements in flow simulations (see, e.g., [3, 21–24]). Nevertheless, we feel the main conclusions have more general applicability, and, in particular, are applicable to low-order finite elements. These are presented in Section 4.

2 Advection-diffusion equation

2.1 Continuous problem

Consider the following time-dependent advection-diffusion equation for ϕ:

$$\mathcal{L}\phi = f \quad \text{in } \Omega, \tag{1}$$

where

$$\mathcal{L}\phi = \frac{\partial \phi}{\partial t} + \boldsymbol{a} \cdot \boldsymbol{\nabla}\phi - \boldsymbol{\nabla} \cdot (\kappa \boldsymbol{\nabla}\phi), \tag{2}$$

in which f is the given source, $\boldsymbol{a}$ is the solenoidal velocity field, κ is the diffusivity, and Ω is the spatial domain of the problem. The essential and natural boundary conditions associated are:

$$\phi = g \quad \text{on } \Gamma_D, \tag{3}$$
$$\kappa \boldsymbol{\nabla}\phi \cdot \boldsymbol{n} = h \quad \text{on } \Gamma_N, \tag{4}$$

where Γ_D and Γ_N are the Dirichlet and Neumann parts of the boundary Γ of the domain Ω, g and h are the prescribed data, and $\boldsymbol{n}$ is the unit outward boundary normal.

Let $\mathcal{V}_g$ and $\mathcal{V}_0$ denote the trial solution and weighting function spaces, respectively, where subscripts g and 0 refer to the essential boundary conditions. The variational counterpart of Eq. (1) reads: find $\phi \in \mathcal{V}_g$ such that $\forall w \in \mathcal{V}_0$,

$$\left(w, \frac{\partial \phi}{\partial t} + \boldsymbol{a} \cdot \boldsymbol{\nabla}\phi\right)_\Omega + (\boldsymbol{\nabla}w, \kappa\boldsymbol{\nabla}\phi)_\Omega = (w, f)_\Omega + (w, h)_{\Gamma_N}, \tag{5}$$

where $(\cdot, \cdot)_\Omega$ and $(\cdot, \cdot)_{\Gamma_N}$ denote the L^2-inner products on Ω and Γ_N, respectively.

2.2 Discrete formulation

Let $\mathcal{V}_g^h$ and $\mathcal{V}_0^h$ be finite-dimensional subspaces of $\mathcal{V}_g$ and $\mathcal{V}_0$, respectively. We state the semi-discrete formulation of the advection-diffusion problem as follows: find $\phi^h \in \mathcal{V}_g^h$ such that $\forall w^h \in \mathcal{V}_0^h$,

$$\left(w^h, \frac{\partial \phi^h}{\partial t} + \boldsymbol{a} \cdot \boldsymbol{\nabla}\phi^h\right)_\Omega + \left(\boldsymbol{\nabla}w^h, \kappa\boldsymbol{\nabla}\phi^h\right)_\Omega - \left(w^h, f\right)_\Omega - \left(w^h, h\right)_{\Gamma_N}$$
$$+ \sum_{e=1}^{n_{el}} \left(\tau\boldsymbol{a} \cdot \boldsymbol{\nabla}w^h, \mathcal{L}\phi^h - f\right)_{\Omega_e} = 0. \tag{6}$$

Variational equation (6) is the SUPG formulation of the advection-diffusion problem [4]. In the sequel we first provide the conventional definitions of the stabilization parameter τ appearing in (6), followed by the EVB definition, first proposed in [1, 2].

2.2.1 Conventional definition of τ's

The following definition of τ is often employed in practice (see, e.g., [3, 25, 26])

$$\tau = (\frac{4}{\Delta t^2} + \boldsymbol{a} \cdot \boldsymbol{G}\boldsymbol{a} + C_I\kappa^2\boldsymbol{G} : \boldsymbol{G})^{-1/2}, \tag{7}$$

where Δt is the time-step size, C_I is a positive constant, independent of the mesh size, derived from the element-wise inverse estimate (see, e.g., [27]),

$$G_{ij} = \sum_{k=1}^3 \frac{\partial \xi_k}{\partial x_i} \frac{\partial \xi_k}{\partial x_j}, \tag{8}$$

$$\boldsymbol{G} : \boldsymbol{G} = \sum_{i,j=1}^3 G_{ij}G_{ij}, \tag{9}$$

$$\boldsymbol{a} \cdot \boldsymbol{G}\boldsymbol{a} = \sum_{i,j=1}^{3} a_i G_{ij} a_j, \tag{10}$$

and $\partial\boldsymbol{\xi}/\partial\boldsymbol{x}$ is the inverse Jacobian of the element mapping between the parametric and physical domains.

Although often employed in practice, τ defined by Eq. (7) is subject to the following criticisms:

(1) Definition (7) is not robust for small time steps. Namely, in the limit of $\Delta t \to 0$, the Δt term becomes dominant and $\tau \to 0$. As a result, formulation (6) reverts to the Galerkin's method, which, in turn, is known to be unstable for the advection-dominated case. As a result, the practitioner is forced to select a time step that is not "too small" to avoid numerical instability associated with the small time step limit.

(2) Definition (7) may not be suitable for steady solutions obtained in time-dependent computations because the steady state depends on Δt through (7).

In view of these remarks, the Δt dependence in τ is sometimes omitted and τ takes on the following definition:

$$\tau = (\boldsymbol{a} \cdot \boldsymbol{G}\boldsymbol{a} + C_I \kappa^2 \boldsymbol{G} : \boldsymbol{G})^{-1/2}. \tag{11}$$

Although favorable in some situations, such as steady solutions, simply omitting Δt from τ may lead to divergent results in practical computations. We will demonstrate this in the numerical examples section of this paper.

2.2.2 Element-vector-based (EVB) τ

Let N_a, $a = 1, \ldots, n_{sh}$, be the element-level basis functions, and n_{sh} be the number of element-level basis functions. Let $(\cdot, \cdot)_{\Omega_e}$ denote the L^2-inner product over the element domain Ω_e corresponding to element e. We define the following element-level vectors:

$$\boldsymbol{c}_V = \{c_a\},$$
$$c_a = \left(N_a, \, \boldsymbol{a} \cdot \boldsymbol{\nabla}\phi^h\right)_{\Omega_e}, \tag{12}$$
$$\tilde{\boldsymbol{k}}_V = \{\tilde{k}_a\},$$
$$\tilde{k}_a = \left(\boldsymbol{a} \cdot \boldsymbol{\nabla}N_a, \, \boldsymbol{a} \cdot \boldsymbol{\nabla}\phi^h\right)_{\Omega_e}, \tag{13}$$
$$\tilde{\boldsymbol{c}}_V = \{\tilde{c}_a\},$$
$$\tilde{c}_a = \left(\boldsymbol{a} \cdot \boldsymbol{\nabla}N_a, \, \frac{\partial\phi^h}{\partial t}\right)_{\Omega_e}. \tag{14}$$

5

The components of the EVB τ are:

$$\tau_1^{-1} = \frac{\|\tilde{\boldsymbol{k}}_V\|}{\|\boldsymbol{c}_V\|}, \tag{15}$$

$$\tau_2^{-1} = \frac{\|\tilde{\boldsymbol{c}}_V\|}{\|\boldsymbol{c}_V\|}, \tag{16}$$

$$\tau_3^{-1} = \tau_1^{-1} Pe^{-1}, \tag{17}$$

where Pe is an element-level Peclet number,

$$Pe = \frac{\|\boldsymbol{a}\|^2}{\kappa} \frac{\|\boldsymbol{c}_V\|}{\|\tilde{\boldsymbol{k}}_V\|}. \tag{18}$$

In equations (15)-(18), $\|\cdot\|$ denotes the l^2-norm. For example, for the vector $\boldsymbol{c}_V$,

$$\|\boldsymbol{c}_V\| = \left(\sum_a c_a^2\right)^{1/2}. \tag{19}$$

We define τ as

$$\tau = \left(\tau_1^{-2} + \tau_2^{-2} + \tau_3^{-2}\right)^{-1/2}. \tag{20}$$

Remarks

(1) The τ_2 term defined in Eq. (16) directly brings in the dependence of τ on the time-step size. In the case when the solution is changing in time, this term is active, while in the steady regime, it is identically zero. As a result, this construction automatically selects a τ appropriate for different solution regimes, making it attractive for practical applications.

(2) The definition of τ given by Eqs. (15)-(20) can be seen as a nonlinear definition because it depends on the solution even in linear problems. However, in marching from time level n to $n + 1$, the element vectors can be evaluated at level n. This eliminates the need of solving a nonlinear discrete system in each time step when the continuous problem is linear.

(3) The definition of τ given by Eqs. (15)-(20) makes τ an element-level constant. One may also define an EVB τ for every global basis function in the formulation by taking a to be a global basis function index and avoiding summation over a's (this option, as well as other variants, were pointed out in [1, 2]). In fact, we may go as far as recommending this technique for computations that employ truly global basis functions, such as spectral methods, where conventional definitions of τ (i.e., (7) and (11)) are not directly applicable due to the global support of the basis functions. However, we note that no experience has yet been gained with methods using global basis functions.

(4) Note that, in contrast to the original references [1, 2], the element Peclet number Pe (see Eq. (18)) is defined using the element vector rather than element

matrix arrays. This is done in the interest of simplicity. It is believed that both definitions will give similar results.

(5) In references [28–30] the authors successfully employed the element-matrix-based variant of τ for compressible flow computations.

(6) Note that the EVB τ was designed using scaling arguments to deliver accuracy comparable to the conventional τ.

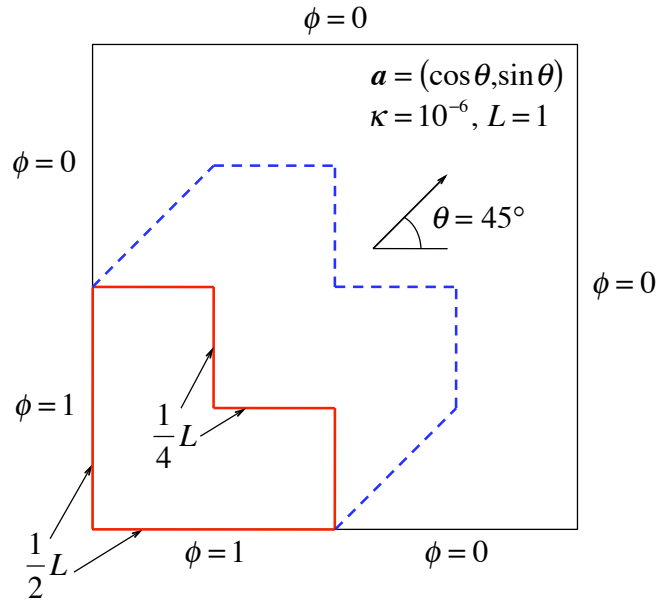## 2.3 Tests with an L-shaped discontinuity advected skew to mesh

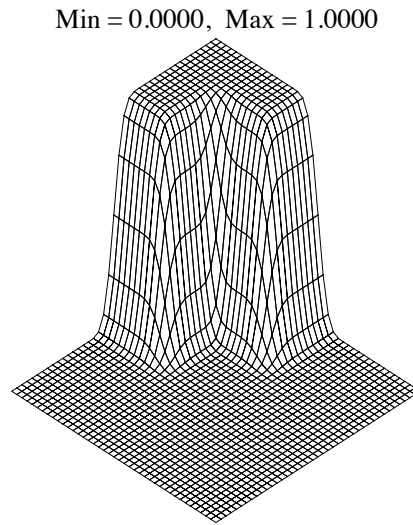Fig. 1. Advection of an L-shaped front. Problem description.

Fig. 2. Advection of an L-shaped front. Elevation plot of the initial condition.

We test the proposed methodology on the advection of an L-shaped front benchmark originally presented in [21]. The problem setup is given in Figure 1. The diffusivity $\kappa = 10^{-6}$, the advection angle is chosen to be 45° and the magnitude of the advective speed is set to unity. The domain is a unit square subdivided into 20×20 square elements. At time $t = 0$ the value of the scalar field is set to unity in the interior of the L-shaped block located in the lower left-hand corner of the domain. Elsewhere in the domain ϕ^h is set to zero, creating an interior layer with an L-shaped concave front as shown in Figure 2. The solution is advanced in time until $t = 0.25$ as well as to the steady state. Given that the diffusion coefficient is very small compared to the advection velocity and the mesh size, for all practical purposes the problem corresponds numerically to pure advection. We will refer to the interior layer as the discontinuity front, and its location and shape at $t = 0.25$ are illustrated in Figure 1 with a dashed line.

We compare solutions produced with conventional τ's defined according to Eqs. (7) and (11) and the EVB version defined according to Eqs. (15)-(20). Both transient and steady-state solutions are considered. C^5-continuous B-splines of degree six are employed for all test cases. Very high-order B-splines have been shown to be especially effective for solutions of the advection-diffusion problem with thin layers (see, e.g., [21, 24]). Time steps $\Delta t = 0.025$, $\Delta t = 0.00625$, and $\Delta t = 0.003125$ are used, the last one being much smaller than what is required for time-accuracy.

Results for all three τ's computed at $\Delta t = 0.025$ are shown in Figures 3 and 4. At this time step the results are similar for all τ's for both transient and steady-state solutions. A small but noticeable "wiggle" is present at the steady state for both the conventional τ with Δt and EVB τ. Nevertheless, the maximum overshoot does not exceed 1.5% and the solution quality is comparable in all cases.

Results for $\Delta t = 0.00625$ are presented in Figures 5 and 6. Transient responses for all three cases are similar. Comparison of the steady-state results for this time step reveals the deficiency for the conventional τ with small Δt: τ is dominated by the Δt term and it is too small to guarantee a stable steady-state solution (see Figure 6(a)). In contrast, both the conventional τ without Δt and the EVB τ deliver nearly identical, stable, and accurate solutions at the steady state.

Results for $\Delta t = 0.003125$ are shown in Figures 7 and 8. At this time step, at $t = 0.25$, the conventional τ with Δt produces small but noticeable wiggles that propagate from the interior layer inward (see Figure 7(a)). At the steady state, at this small time step, the effect of the Δt term in the conventional definition of τ leads to significant oscillations (see Figure 8(a)), where stability is achieved for the conventional τ without Δt and the EVB τ. There are, once again, small oscillations for the EVB τ.

For this problem, the conventional τ without Δt generates solutions of somewhat better quality than the EVB τ. However, as will be shown in the sequel, the con-

Min = -0.0054, Max = 1.0320   Min = -0.0054, Max = 1.0299   Min = -0.0070, Max = 1.0285

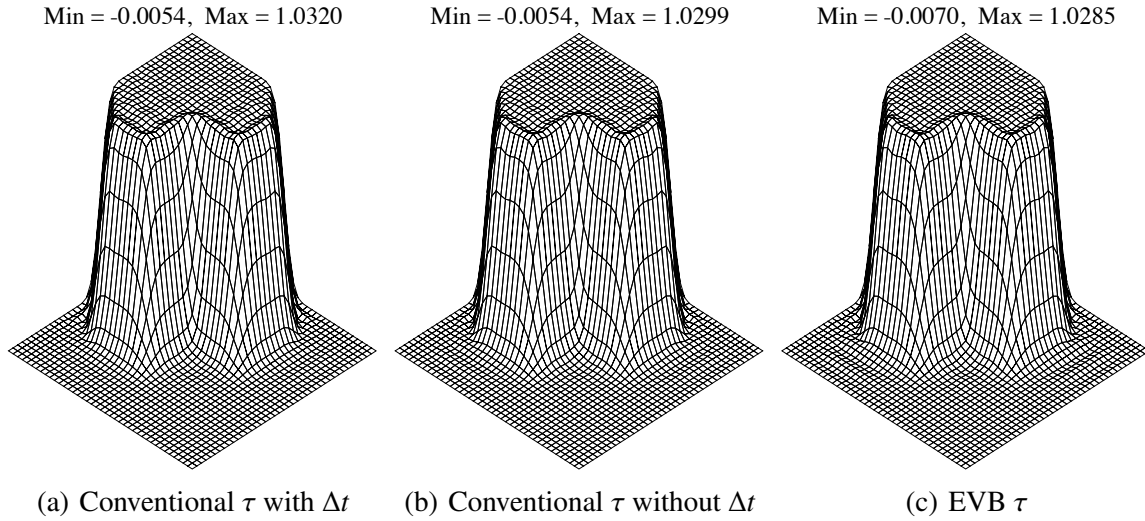(a) Conventional τ with Δt (b) Conventional τ without Δt (c) EVB τ

Fig. 3. Advection of an L-shaped front. Results using C^5-continuous splines of order six. Elevation plot of the transient solution (interpolated with 40×40 bilinear elements) at $t = 0.25$ with $\Delta t = 0.025$
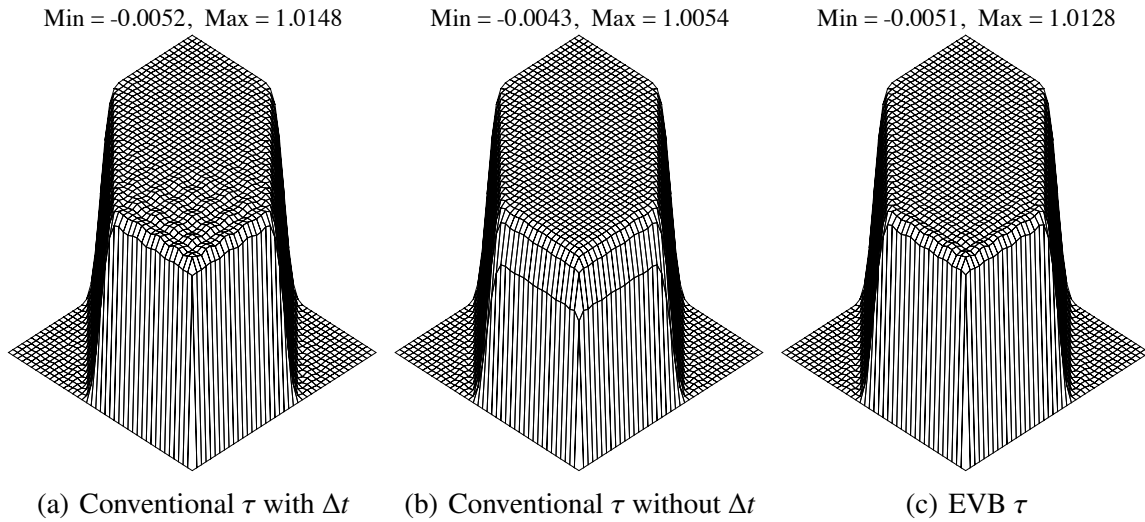

Min = -0.0052, Max = 1.0148   Min = -0.0043, Max = 1.0054   Min = -0.0051, Max = 1.0128

(a) Conventional τ with Δt (b) Conventional τ without Δt (c) EVB τ

Fig. 4. Advection of an L-shaped front. Results using C^5-continuous splines of order six. Elevation plot of the steady-state solution (interpolated with 40×40 bilinear elements) with $\Delta t = 0.025$.

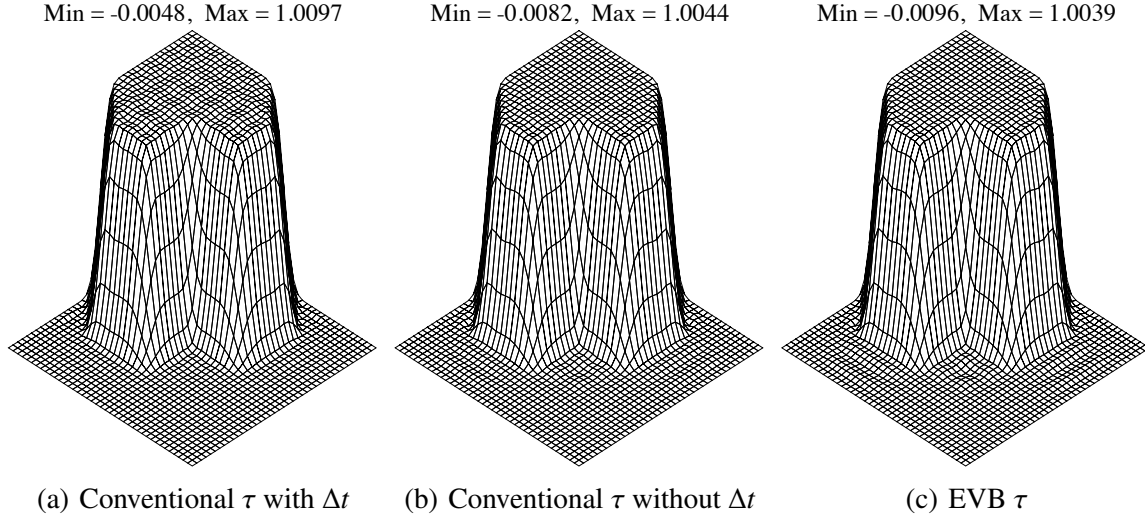ventional definition of τ without Δt is not sufficiently robust in more complicated situations.

9

Min = -0.0048, Max = 1.0097   Min = -0.0082, Max = 1.0044   Min = -0.0096, Max = 1.0039

(a) Conventional τ with Δt (b) Conventional τ without Δt (c) EVB τ

Fig. 5. Advection of an L-shaped front. Results using C^5-continuous splines of order six. Elevation plot of the transient solution (interpolated with 40×40 bilinear elements) at $t = 0.25$ with $\Delta t = 0.00625$.
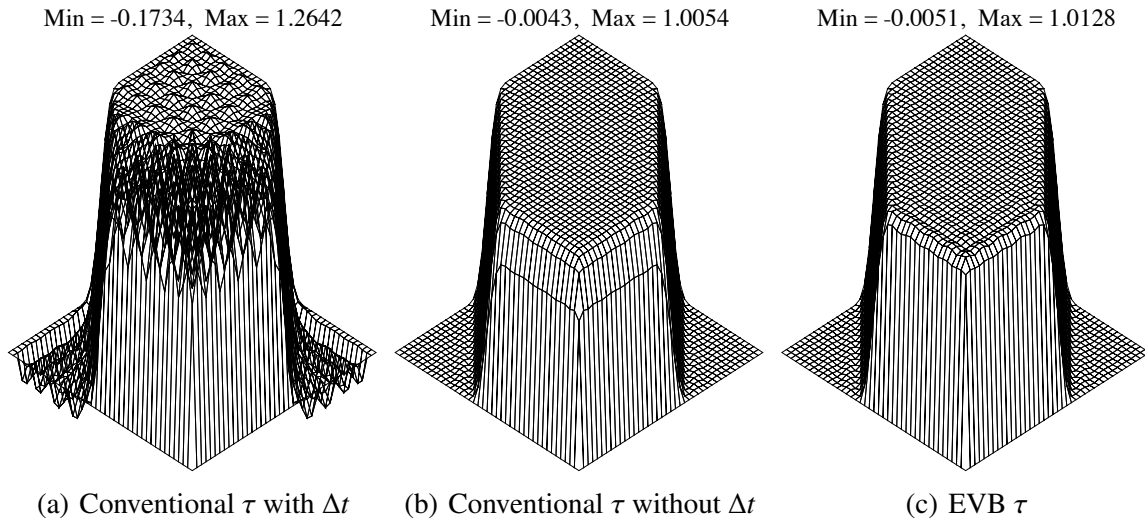
Min = -0.1734, Max = 1.2642   Min = -0.0043, Max = 1.0054   Min = -0.0051, Max = 1.0128

(a) Conventional τ with Δt (b) Conventional τ without Δt (c) EVB τ

Fig. 6. Advection of an L-shaped front. Results using C^5-continuous splines of order six. Elevation plot of the steady-state solution (interpolated with 40×40 bilinear elements) with $\Delta t = 0.00625$.

3 Variational multiscale residual-based turbulence modeling

In this section we adapt the definition of the EVB τ's to the incompressible Navier-Stokes equations and make use of them in the context of the variational multiscale residual-based turbulence modeling (see [3]). EVB τ's for stabilized formulations of the incompressible Navier-Stokes equations were first proposed in [1, 2].
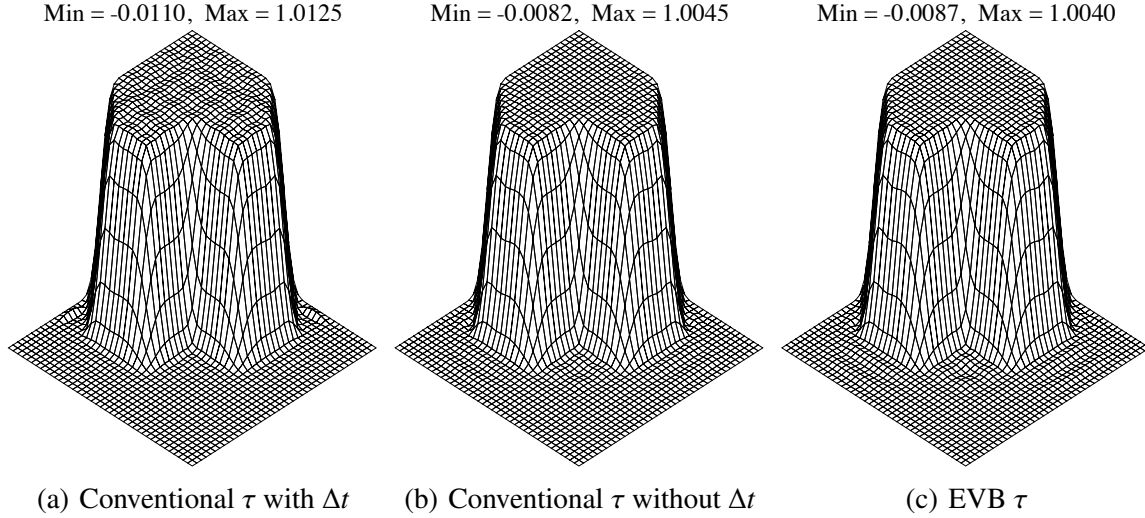
Min = -0.0110, Max = 1.0125   Min = -0.0082, Max = 1.0045   Min = -0.0087, Max = 1.0040

(a) Conventional τ with Δt (b) Conventional τ without Δt (c) EVB τ

Fig. 7. Advection of an L-shaped front. Results using C^5-continuous splines of order six. Elevation plot of the transient solution (interpolated with 40×40 bilinear elements) at $t = 0.25$ with $\Delta t = 0.003125$.
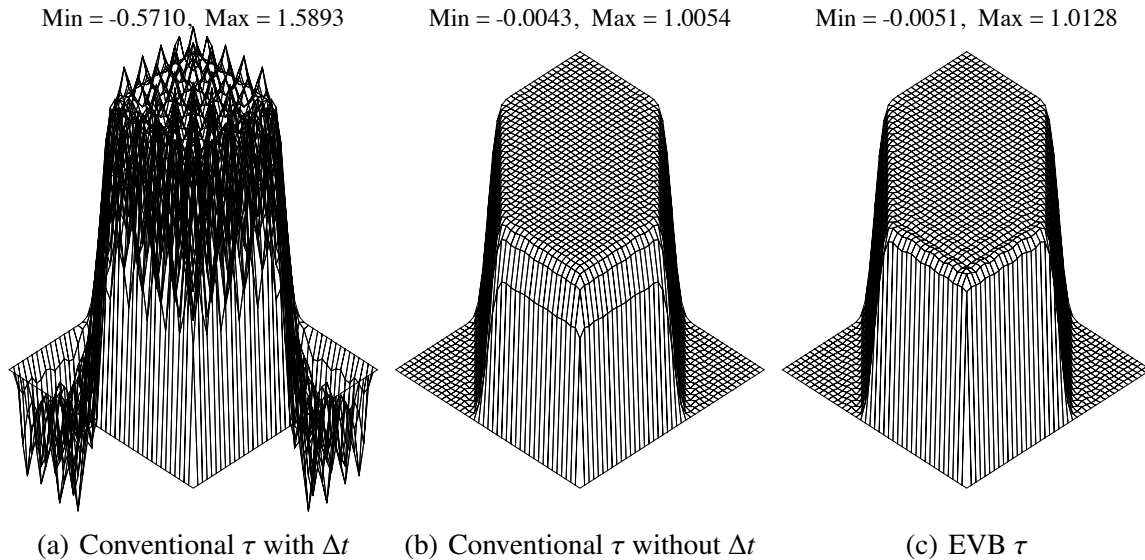
Min = -0.5710, Max = 1.5893   Min = -0.0043, Max = 1.0054   Min = -0.0051, Max = 1.0128

(a) Conventional τ with Δt (b) Conventional τ without Δt (c) EVB τ

Fig. 8. Advection of an L-shaped front. Results using C^5-continuous splines of order six. Elevation plot of the steady-state solution (interpolated with 40×40 bilinear elements) with $\Delta t = 0.003125$.

3.1 Continuous problem

We begin by considering a weak formulation of the incompressible Navier-Stokes equations. Let $\mathcal{V}$ represent both the trial solution and weighting function spaces, which are assumed to be the same (we assume for simplicity of exposition that $\boldsymbol{u} = \boldsymbol{0}$ on Γ). We also assume that $\int_{\Omega} p(t) d\Omega = 0$ for all $t \in]0, T[$. As before,

11

$(\cdot, \cdot)_\Omega$ denotes the L^2-inner product with respect to the domain Ω. The variational formulation is stated as follows: find $U = \{u, p\} \in V$ such that $\forall W = \{w, q\} \in V$,

$$B(W, U) = L(W), \tag{21}$$

where

$$B(W, U) = \left(w, \frac{\partial u}{\partial t}\right)_\Omega - (\nabla w, u \otimes u)_\Omega - (\nabla \cdot w, p)_\Omega + (q, \nabla \cdot u)_\Omega$$
$$+ (\nabla^s w, 2\nu \nabla^s u)_\Omega, \tag{22}$$
$$L(W) = (w, f)_\Omega, \tag{23}$$

and

$$\nabla^s u = \frac{1}{2}\left(\nabla u + \nabla u^T\right). \tag{24}$$

Here, f is the given body force (per unit mass), ν is the kinematic viscosity and p is the pressure divided by the density.

Variational equations (21)-(23) imply weak satisfaction of the linear momentum equations and incompressibility constraint, namely

$$\frac{\partial u}{\partial t} + \nabla \cdot (u \otimes u) + \nabla p - \nabla \cdot (2\nu \nabla^s u) - f = 0 \quad \text{in } \Omega, \tag{25}$$
$$\nabla \cdot u = 0 \quad \text{in } \Omega. \tag{26}$$

3.2 Discrete formulation

Below, we recall the discrete variational formulation of the incompressible Navier-Stokes equations (see [3]). We approximate Eqs. (21)-(23) by the following variational problem over the finite-element spaces: find $U^h = \{u^h, p^h\} \in V^h$ such that $\forall W^h = \{w^h, q^h\} \in V^h$,

$$B\left(W^h, U^h\right) + \left(u^h \cdot \nabla w^h + \nabla q^h, \tau_M r_M\right)_\Omega + \left(\nabla \cdot w^h, \tau_C r_C\right)_\Omega$$
$$+ \left((\nabla w^h)^T u^h, \tau_M r_M\right)_\Omega - \left(\nabla w^h, \tau_M r_M \otimes \tau_M r_M\right)_\Omega = L\left(W^h\right), \tag{27}$$

where

$$r_M\left(u^h, p^h\right) = \frac{\partial u^h}{\partial t} + u^h \cdot \nabla u^h + \nabla p^h - \nu \Delta u^h - f, \tag{28}$$
$$r_C\left(u^h\right) = \nabla \cdot u^h. \tag{29}$$

Remarks

(1) This is a residual-based variational multiscale method for incompressible Navier-Stokes equations (see [3]). For background, see, e.g., [25, 31–35]. The first term on the left-hand side of Eq. (27) is the Galerkin term; the next two terms are classical stabilization terms; and the last two terms are the additional terms produced by the variational multiscale method.

(2) Note that in the definition of the momentum residual given by Eq. (28), we applied the incompressibility constraint to the advective and the viscous stress terms. As a result, the advective term appears in the convection form, while the viscous stress term appears in the Laplacian form (i.e., compare Eqs. (25) and (28)). Computational experience indicates that this form is more favorable for the stability of the discrete formulation.

3.2.1 Conventional definition of τ's

We recall the conventional definition of τ_M that is commonly employed in practice and is form-identical to Eq. (7):

$$\tau_M = \left(\frac{4}{\Delta t^2} + \boldsymbol{u}^h \cdot \boldsymbol{G}\boldsymbol{u}^h + C_I \nu^2 \boldsymbol{G} : \boldsymbol{G} \right)^{-1/2}. \tag{30}$$

In Eq. (27), τ_C is given as

$$\tau_C = (\tau_M \boldsymbol{g} \cdot \boldsymbol{g})^{-1}. \tag{31}$$

This definition of τ_C comes from the small-scale Shur complement operator for the pressure (see [36]). In Eq. (31), $\boldsymbol{g}$ is a vector obtained by summing $\partial \boldsymbol{\xi}/\partial \boldsymbol{x}$ on its first index as

$$g_i = \sum_{j=1}^{3} \frac{\partial \xi_j}{\partial x_i}, \tag{32}$$

$$\boldsymbol{g} \cdot \boldsymbol{g} = \sum_{i=1}^{3} g_i g_i. \tag{33}$$

As in the previous section on the time-dependent advection-diffusion equation, we also consider τ_M in which the dependence on the time-step size is omitted, that is,

$$\tau_M = \left(\boldsymbol{u}^h \cdot \boldsymbol{G}\boldsymbol{u}^h + C_I \nu^2 \boldsymbol{G} : \boldsymbol{G} \right)^{-1/2}. \tag{34}$$

3.2.2 EVB τ's for the incompressible Navier-Stokes equations

We use the notation of the previous section. In addition, let $\boldsymbol{e}_i$ be the ith Cartesian basis vector. We define the following element-level vectors:

$$\boldsymbol{c}_V = [c_{a,i}],$$

13

$$c_{a,i} = \left(N_a \boldsymbol{e}_i, \ \boldsymbol{u}^h \cdot \boldsymbol{\nabla}\boldsymbol{u}^h\right)_{\Omega_e}, \tag{35}$$

$$\tilde{\boldsymbol{k}}_V = \left[\tilde{k}_{a,i}\right],$$

$$\tilde{k}_{a,i} = \left(\boldsymbol{u}^h \cdot \boldsymbol{\nabla}N_a \boldsymbol{e}_i, \ \boldsymbol{u}^h \cdot \boldsymbol{\nabla}\boldsymbol{u}^h\right)_{\Omega_e}, \tag{36}$$

$$\tilde{\boldsymbol{k}}_V^r = \left[\tilde{k}_{a,i}^r\right],$$

$$\tilde{k}_{a,i}^r = \left(\boldsymbol{r} \cdot \boldsymbol{\nabla}N_a \boldsymbol{e}_i, \ \boldsymbol{r} \cdot \boldsymbol{\nabla}\boldsymbol{u}^h\right)_{\Omega_e}, \tag{37}$$

$$\tilde{\boldsymbol{c}}_V = \left[\tilde{c}_{a,i}\right],$$

$$\tilde{c}_{a,i} = \left(\boldsymbol{u}^h \cdot \boldsymbol{\nabla}N_a \boldsymbol{e}_i, \ \frac{\partial \boldsymbol{u}^h}{\partial t}\right)_{\Omega_e}. \tag{38}$$

In Eq. (37), $\boldsymbol{r}$ is the unit vector in the direction of the solution absolute value gradient,

$$\boldsymbol{r} = \frac{\boldsymbol{\nabla}\|\boldsymbol{u}^h\|}{\left\|\boldsymbol{\nabla}\|\boldsymbol{u}^h\|\right\|}. \tag{39}$$

The three components of the EVB τ are:

$$\tau_1^{-1} = \frac{\|\tilde{\boldsymbol{k}}_V\|}{\|\boldsymbol{c}_V\|}, \tag{40}$$

$$\tau_2^{-1} = \frac{\|\tilde{\boldsymbol{c}}_V\|}{\|\boldsymbol{c}_V\|}, \tag{41}$$

$$\tau_3^{-1} = \tau_1^{-1}\frac{\nu\|\tilde{\boldsymbol{k}}_V^r\|}{\|\boldsymbol{c}_V\|}. \tag{42}$$

We define τ_M as

$$\tau_M = \left(\tau_1^{-2} + \tau_2^{-2} + \tau_3^{-2}\right)^{-1/2}. \tag{43}$$

Remarks

(1) In Eqs. (40)-(42), as before, $\|\cdot\|$ is used to denote the vector l^2-norm, that is, for the vector $\boldsymbol{c}_V$,

$$\|\boldsymbol{c}_V\| = \left(\sum_{a,i} c_{a,i}^2\right)^{1/2}. \tag{44}$$

(2) In Eq. (37), $\tilde{\boldsymbol{k}}_V^r$ is introduced for boundary layer flows. Near solid boundaries, the vector $\boldsymbol{r}$ points in the direction orthogonal to the solid wall, and, as a result, for boundary layer elements with high aspect ratios, the EVB τ switches to the viscous limit with the mesh size h corresponding to the element wall-normal dimension.

14

(3) The equation for τ_C remains unchanged (see Eq. (31)), although τ_M employed in its definition now comes from Eq. (43).

(4) Unlike in the original references [1, 2], we make use of a purely vector-based definition for τ_3 in Eq. (42). This is done in the interest of simplicity and is well suited for matrix-free computations (not employed in this work).

(5) The τ_M does not depend on the pressure and is not the same as the EVB τ_M for the Navier-Stokes equations proposed by [1, 2]. As such, the present EVB τ_M will have a different Stokes limit. This is an issue that is not studied here, but warrants further investigation.

3.3 Laminar flow in a square domain at low Reynolds number

$$u = u|_\Gamma$$

$$u = \begin{Bmatrix} \sin(\pi x - 0.7)\sin(\pi y + 0.2) \\ \cos(\pi x - 0.7)\cos(\pi y + 0.2) \end{Bmatrix}$$

$$p = \sin(x)\cos(y) + (\cos(1) - 1)\sin(1)$$

$$f = \begin{Bmatrix} \cos(x)\cos(y) + \pi\sin(\pi x - 0.7)\cos(\pi x - 0.7) \\ \qquad +2\pi^2\sin(\pi x - 0.7)\sin(\pi y + 0.2) \\ -\sin(x)\sin(y) - \pi\sin(\pi y + 0.2)\cos(\pi y + 0.2) \\ \qquad +2\pi^2\cos(\pi x - 0.7)\cos(\pi y + 0.2) \end{Bmatrix}$$

$$v = 1.0$$

$$u = u|_\Gamma \qquad\qquad u = u|_\Gamma$$

$$L = 1 \qquad\qquad u = u|_\Gamma$$

Fig. 9. Laminar flow in a square domain at low Reynolds number. Problem description.

The small time step problem also appears when stabilized rather than BB-stable formulations are employed for the time-dependent Stokes (see e.g., [37, 38]) as well as low Reynolds number Navier-Stokes (see [16]) problems. To examine the performance of the different τ's in this regime, we consider a test case originally proposed in [38] in the context of the Stokes equations, and solved in [16] using the Navier-Stokes equations. We consider the latter case. The problem's setup and its analytical solution are presented in Figure 9.

We solve the problem using Dirichlet boundary conditions on the velocity field. The velocity boundary condition is obtained as follows: we perform an L_2 projection of the analytical velocity solution onto our discrete space, which consists of C^1-continuous quadratic B-splines. The control variables at the domain boundary are assigned Dirichlet boundary conditions with values that come from the L_2 projection. To assign the initial conditions, we set the velocity to zero in the domain

15

interior and the pressure to zero everywhere in the domain, including the boundary. We use a uniform mesh of 80×80 elements.

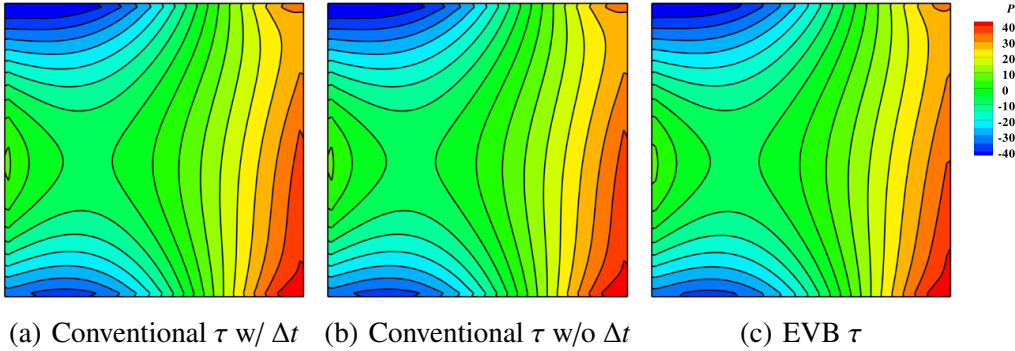(a) Conventional τ w/ Δt (b) Conventional τ w/o Δt (c) EVB τ

Fig. 10. Laminar flow in a square domain at low Reynolds number. Pressure contours of the solution at the first time step for $\Delta t = 0.01$. The initial conditions are: zero velocity in the domain interior and zero pressure everywhere.
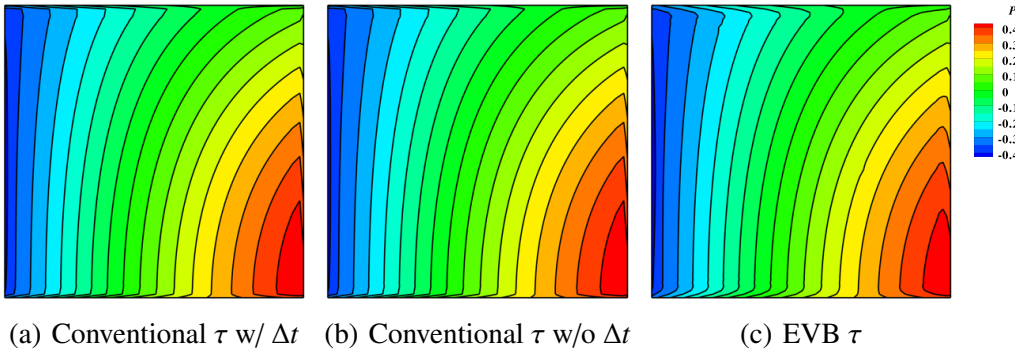

(a) Conventional τ w/ Δt (b) Conventional τ w/o Δt (c) EVB τ

Fig. 11. Laminar flow in a square domain at low Reynolds number. Contours of the steady-state pressure solution for $\Delta t = 0.01$.

We solve the problem at the large time step of $\Delta t = 0.01$ using all three definitions of τ. The fluid pressure is shown in Figures 10 and 11, which correspond to the solution at the end of the first time step and the steady-state solution, respectively. In all cases the solutions are stable. At the steady state, in the interior of the domain, the discrete pressure solution is very close to its analytical counterpart. However, at the domain boundary, the pressure solution develops a boundary layer, which is a well-known artifact that occurs in stabilized formulations of Stokes equations as well as Navier-Stokes equations in the low Reynolds number regime. (See [39] for an explanation of this phenomenon and a simple remedy, which was not implemented in this work.)

The sensitivity of the three formulations to small time steps is studied as follows. We take the steady-state solution from the large time step of $\Delta t = 0.01$ as the initial condition for the simulation at $\Delta t = 0.000001$. This is the smallest time step employed in [16, 38]. This procedure of starting with the initial conditions that are close to the steady-state solution of the underlying equations is similar to
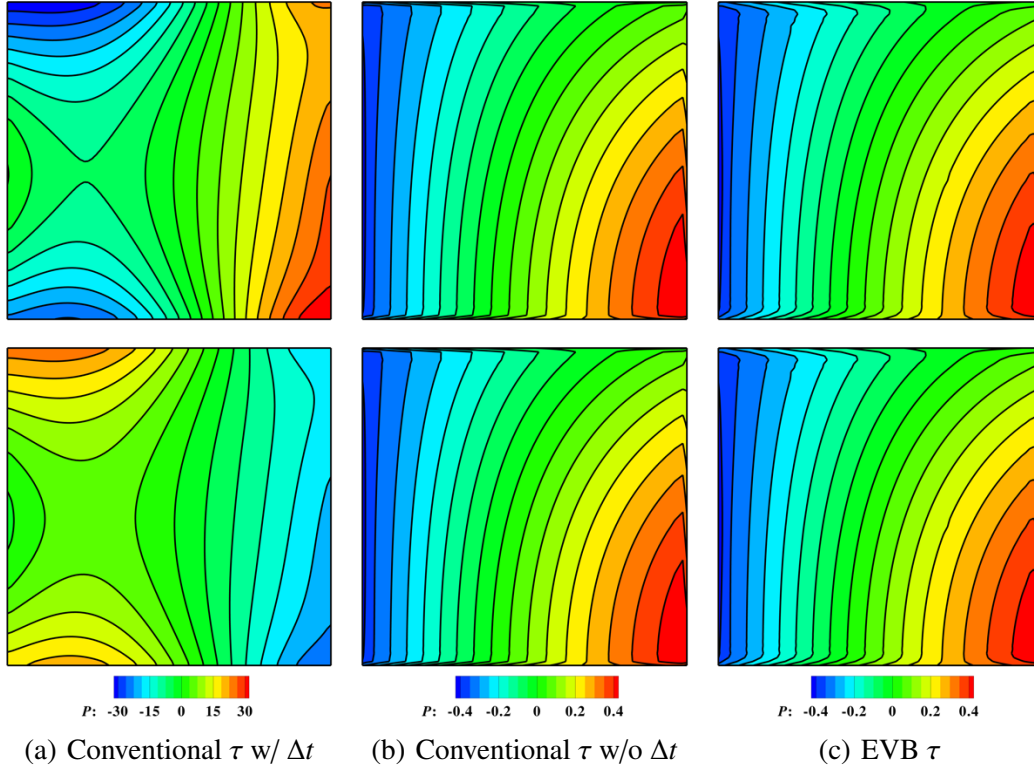
(a) Conventional τ w/ Δt (b) Conventional τ w/o Δt (c) EVB τ

Fig. 12. Laminar flow in a square domain at low Reynolds number. Pressure contours of the first- and second-step solutions for $\Delta t = 0.000001$. The initial conditions are set to be the steady-state solution from $\Delta t = 0.01$.
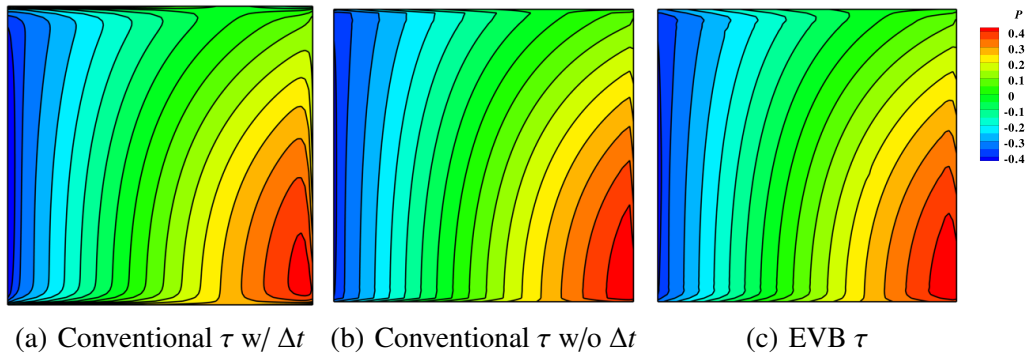

(a) Conventional τ w/ Δt (b) Conventional τ w/o Δt (c) EVB τ

Fig. 13. Laminar flow in a square domain at low Reynolds number. Contours of the steady-state pressure solution for $\Delta t = 0.000001$.

that employed in [16]. The expected result is that the solution does not change, that is, the steady state results are not sensitive to the definition of the stabilization parameter. Figure 12 shows the pressure solution for the first two time steps for all methods considered. The solution remains nearly identical to the initial condition for the cases of the EVB τ and conventional τ without Δt. On the other hand, for the conventional τ with Δt, the pressure solution rapidly departs from the initial condition, which means that the steady-state solution is sensitive to this definition of the stabilization parameter. Also note that the pressure changes sign from the first

17

to the second time step, indicating oscillatory-in-time behavior. Despite the rapid transient in the case of the conventional τ with Δt, the solution reaches a steady state that is very similar to that of the other τ definitions (see Figure 13).

Remarks

(1) Despite the sensitivity to the time step size, no spatial pressure instability was observed for any of the three τ definitions. Even in the case of the small time step and the conventional τ with Δt, the transient pressure solution remained smooth. This is in contrast to the results of [16, 38], and may be attributable to the differences in the spatial discretization used here and in the aforementioned references.

(2) We would also like to point out that in [2] the authors used τ_M defined in Eq. (43) on the test problem of vortex shedding about a circular cylinder at low Reynolds number $Re = 100$. Because of the non-uniformity of the mesh used, the local Courant number (i.e. the normalized time-step size) varied from approximately 1.0 to as small as 0.04. The results showed that even at such small time steps, the element-vector-based τ was stable and yielded an accurate solution.

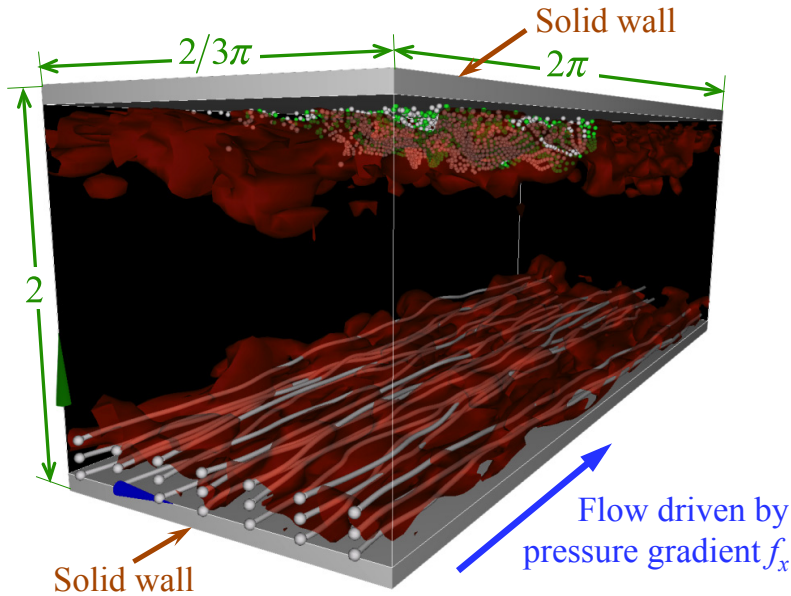### 3.4   Turbulent channel flow at $Re_\tau = 395$

Fig. 14. Turbulent channel flow. Problem setup.

Our last numerical example is an equilibrium turbulent channel flow at Reynolds number 395 based on the friction velocity and channel half-width. The problem setup is shown in Figure 14.The computational domain is a rectangular box of size

$2\pi \times 2 \times \frac{2}{3}\pi$ in the stream-wise, wall-normal, and span-wise directions, respectively. A no-slip Dirichlet boundary condition is set at the wall ($y = \pm 1$), while the stream-wise and the span-wise directions are assigned periodic boundary conditions. The flow is driven by a constant pressure gradient, f_x, acting in the stream-wise direction. The values of the kinematic viscosity ν and the forcing f_x are set to 1.472×10^{-4} and 3.37204×10^{-3}, respectively, which results in a bulk stream-wise velocity of unity.

The computations are performed on a mesh of 32^3 elements and the mesh is graded in the wall-normal direction to better capture the boundary layer. For the spatial discretization we employ isogeometric analysis (see, e.g., [3, 22, 24, 40]) and C^1-continuous quadratic B-splines are considered for this test case. Numerical results are reported in the form of statistics of the mean velocity and root-mean-square velocity fluctuations. Statistics are obtained by sampling the solution field at the mesh knots and averaging in the stream-wise and span-wise directions as well as in time. Comparison of the statistical quantities of interest with the DNS data of Moser *et al.* [41] is made in order to assess the accuracy and robustness of the proposed procedure. All the results are presented in non-dimensional wall units.

We compare the numerical results obtained using the conventional definition of τ_M, with and without the Δt term, and the EVB definition of τ_M. We consider five time step sizes: $\Delta t = 0.1$, $\Delta t = 0.025$, $\Delta t = 0.00625$, $\Delta t = 0.0015625$ and $\Delta t = 0.000390625$. Figure 15 corresponds to the simulation at $\Delta t = 0.1$. At this large time step the solutions are very similar for all τ_M's, while the conventional τ_M with the Δt term showing a slightly more accurate mean flow result.

We note that $\Delta t = 0.1$ is the only time step out of the five considered for which we were able to generate a numerical solution using the conventional τ_M without Δt. For all other time steps we observed rapid divergence with this τ_M. It is now well known from numerous test computations carried out by different researchers that some problems require the inclusion of the transient term in the expression for τ_M and some problems require the exclusion of this term. The turbulent channel flow is a problem that requires the inclusion of the Δt term, and hence formulation (34) fails to produce a convergent solution for time step sizes smaller than $\Delta t = 0.1$.

In Figure 16 we compare the solutions obtained with the conventional τ_M with Δt for the four time-step sizes. Stable solutions are obtained for all time step sizes, and for larger time steps are very similar, but the accuracy of the results deteriorates for smaller time steps. This is especially evident for the mean flow and stream-wise fluctuation. The results for the EVB τ_M are presented in Figure 17. The results for all time steps are nearly identical and, in particular, no deterioration of accuracy with decreasing time step size is observed.
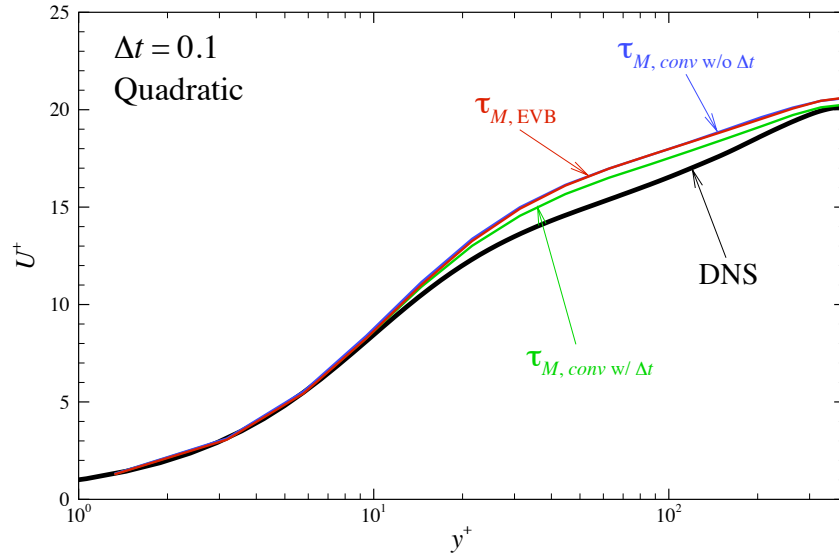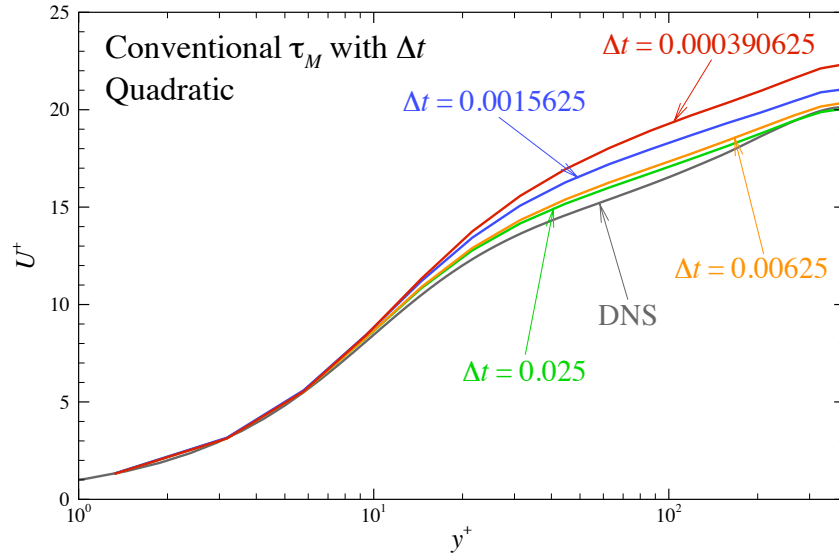
(a) Mean stream-wise velocity
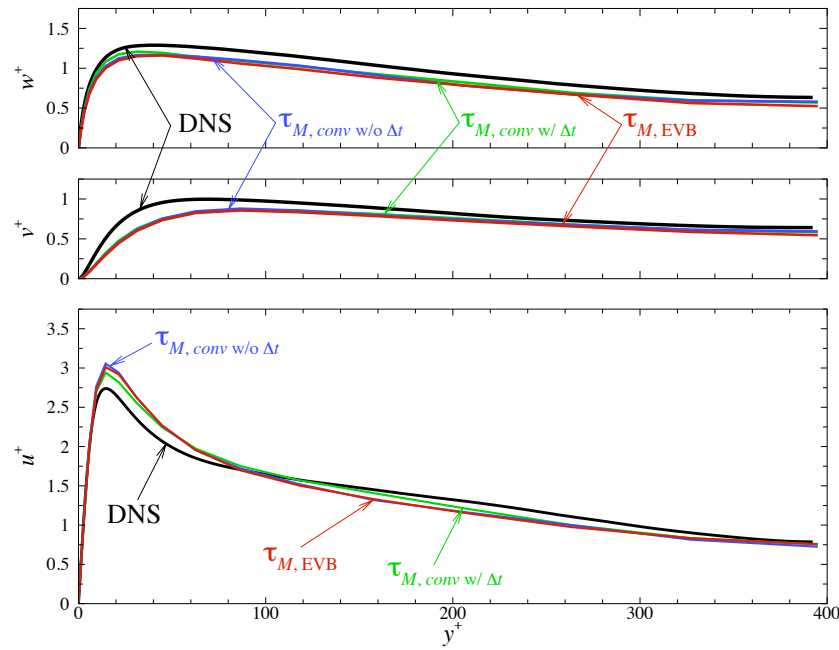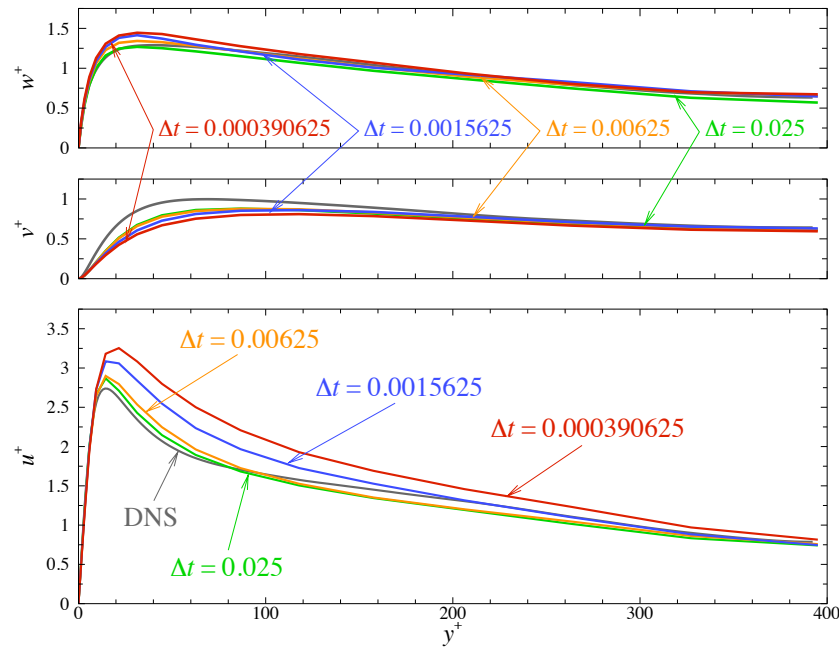

(b) Velocity fluctuations

Fig. 15. Turbulent channel flow at Re_τ = 395 using quadratic NURBS. Results computed at Δt = 0.1 using the conventional τ_M with and without Δt, and the EVB τ_M.

4 Conclusions

We have numerically studied the behavior of element-vector-based (EVB) stabilization parameters in stabilized/variational multiscale formulations of the time-dependent linear advection-diffusion and incompressible Navier-Stokes equations.
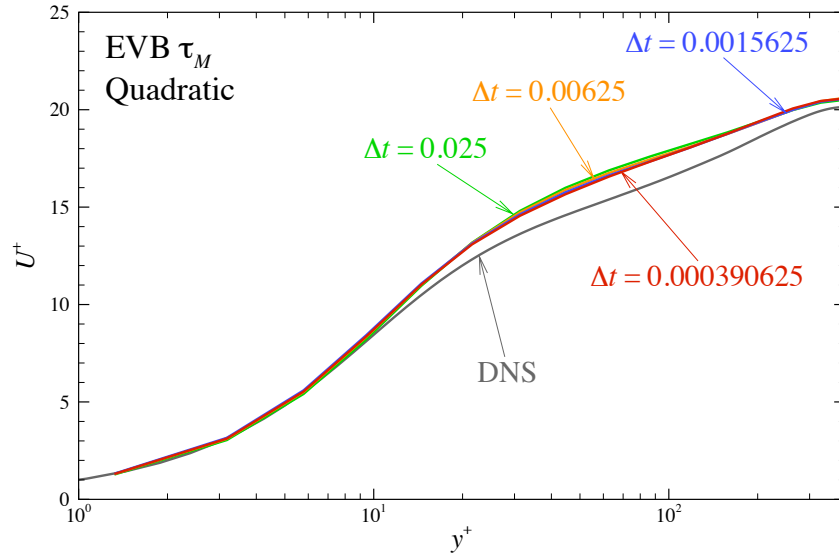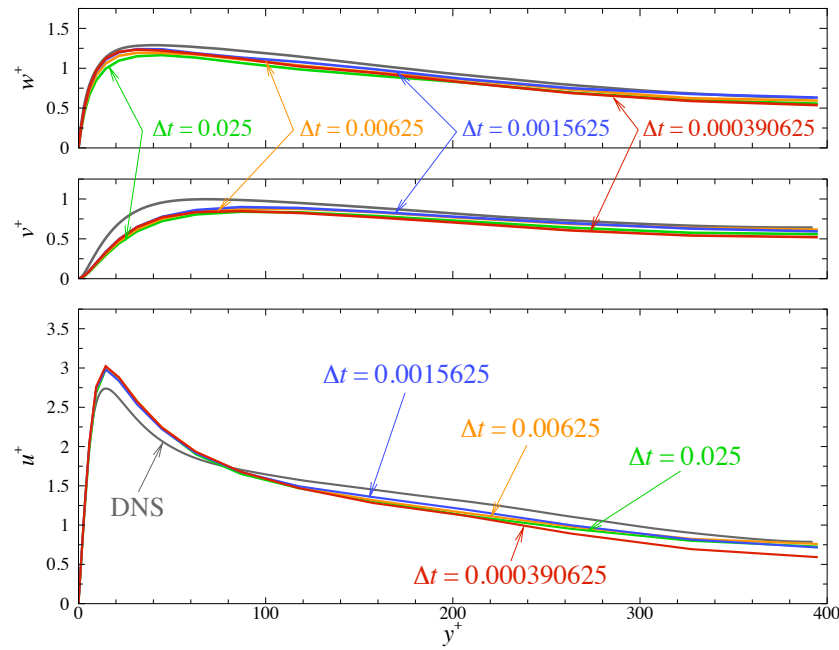
20

(a) Mean stream-wise velocity

(b) Velocity fluctuations

Fig. 16. Turbulent channel flow at $Re_\tau = 395$ using quadratic NURBS. Results using conventional τ_M with Δt for $\Delta t = 0.025$, $\Delta t = 0.00625$, $\Delta t = 0.0015625$ and $\Delta t = 0.000390625$.

In comparison with conventional definitions of stabilization parameters, when the conventional definitions yield stable results, the EVB parameters yielded comparable accuracy, sometimes slightly worse, sometimes slightly better. However, the conventional definitions that depend on the time step yield instabilities at small time steps, and the conventional definitions that do not depend on the time step

(a) Mean stream-wise velocity

(b) Velocity fluctuations

Fig. 17. Turbulent channel flow at $Re_\tau = 395$ using quadratic NURBS. Results using EVB τ_M for $\Delta t = 0.025$, $\Delta t = 0.00625$, $\Delta t = 0.0015625$ and $\Delta t = 0.000390625$.

yield instabilities in complex, time-dependent flows, such as the turbulent channel flow, whereas the EVB definitions behaved robustly in all cases studied. At large time steps, all approaches seem to be more or less equivalent. These findings are consistent with earlier cases in [1, 2].

The shortcomings of the EVB procedure are that no stability analysis is available

to validate it theoretically and it introduces a nonlinearity in otherwise linear problems. With respect to these shortcomings, the dynamic subgrid scales approach of Codina *et al.* [16] is superior. However, the EVB procedure has some attributes, namely, it is simply implemented in existing stabilized/variational multiscale computer programs, it does not entail the solution of an evolution equation for the small scales and this avoids the storage of small scales as history variables, and it provides a fair combination of accuracy and robustness in contrast with conventional definitions. We understand the approach is ad hoc and we do not believe it is the ultimate solution to the definition of small-scales in stabilized and variational multiscale methods, but based on our results and others we know of [1, 2], it appears to be a simple, effective and practically useful option. When things work, they usually work for a reason. Is there a fundamental basis of the EVB procedure? This is an intriguing question that can only be answered by future research.

References

[1] T.E. Tezduyar. Computation of moving boundaries and interfaces and stabilization parameters. *International Journal for Numerical Methods in Fluids*, 43:555–575, 2003.

[2] T.E. Tezduyar and Y. Osawa. Finite element stabilization parameters computed from element matrices and vectors. *Computer Methods in Applied Mechanics and Engineering*, 190:411–430, 2000.

[3] Y. Bazilevs, V.M. Calo, J.A. Cottrel, T.J.R. Hughes, A. Reali, and G. Scovazzi. Variational multiscale residual-based turbulence modeling for large eddy simulation of incompressible flows. *Computer Methods in Applied Mechanics and Engineering*, 197:173–201, 2007.

[4] A.N. Brooks and T.J.R. Hughes. Streamline upwind/Petrov-Galerkin formulations for convection dominated flows with particular emphasis on the incompressible Navier-Stokes equations. *Computer Methods in Applied Mechanics and Engineering*, 32:199–259, 1982.

[5] T.J.R. Hughes and M. Mallet. A new finite element formulation for fluid dynamics: III. The generalized streamline operator for multidimensional advective-diffusive systems. *Computer Methods in Applied Mechanics and Engineering*, 58:305–328, 1986.

[6] F. Shakib, T.J.R. Hughes, and Z. Johan. A new finite element formulation for computational fluid dynamics: X. The compressible Euler and Navier-Stokes equations. *Computer Methods in Applied Mechanics and Engineering*, 89:141–219, 1991.

[7] T.J.R Hughes and T.E. Tezduyar. Finite element methods for first-order hyperbolic systems with particular emphasis on the compressible Euler equations. *Computer Methods in Applied Mechanics and Engineering*, 45:217–284, 1984.

[8] T.E. Tezduyar and Y.J. Park. Discontinuity capturing finite element formulations for nonlinear convection-diffusion-reaction equations. *Computer Methods in Applied Mechanics and Engineering*, 59:307–325, 1986.

[9] T.E. Tezduyar. Finite element methods for fluid dynamics with moving boundaries and interfaces. In E. Stein, R. de Borst, and T.J.R. Hughes, editors, *Encyclopedia of Computational Mechanics, Volume 3: Fluids*, chapter 17. John Wiley & Sons, Ltd, 2004.

[10] T.J.R. Hughes, V.M. Calo, and G. Scovazzi. Variational and multiscale methods in turbulence. In W. Gutkowski and T.A. Kowalewski, editors, *In Proceedings of the XXI International Congress of Theoretical and Applied Mechanics (IUTAM)*. Kluwer, 2004.

[11] V.M. Calo. *Residual-based Multiscale Turbulence Modeling: Finite Volume Simulation of Bypass Transistion*. PhD thesis, Department of Civil and Environmental Engineering, Stanford University, 2004.

[12] T.E. Tezduyar and M. Senga. Stabilization and shock-capturing parameters in SUPG formulation of compressible flows. *Computer Methods in Applied Mechanics and Engineering*, 195:1621–1632, 2006.

[13] T.J.R. Hughes and G. Sangalli. Variational multiscale analysis: the fine-scale Green's function, projection, optimization, localization, and stabilized methods. *SIAM Journal of Numerical Analysis*, 45:539–557, 2007.

[14] I. Harari. Stability of semidiscrete formulations for parabolic problems at small time steps. *Computer Methods in Applied Mechanics and Engineering*, 193:1491–1516, 2004.

[15] I. Harari and G. Hauke. Semidiscrete formulations for transient transport at small time steps. *International Journal for Numerical Methods in Fluids*, 54:731–743, 2007.

[16] R. Codina, J. Principe, O. Guasch, and S. Badia. Time dependent subscales in the stabilized finite element approximation of incompressible flow problems. *Computer Methods in Applied Mechanics and Engineering*, 196:2413–2430, 2007.

[17] J.C. Simo and T.J.R. Hughes. *Computational Inelasticity*. Springer-Verlag, New York, 1998.

[18] G. Houzeaux and J. Principe. A variational subgrid scale model for transient incompressible flows. *International Journal of Computational Fluid Dynamics*, 22:135–152, 2008.

[19] J. Chung and G.M. Hulbert. A time integration algorithm for structural dynamics with improved numerical dissipation: The generalized-α method.

Journal of Applied Mechanics, 60:371–75, 1993.

[20] K.E. Jansen, C.H. Whiting, and G.M. Hulbert. A generalized-α method for integrating the filtered Navier-Stokes equations with a stabilized finite element method. *Computer Methods in Applied Mechanics and Engineering*, 190:305–319, 1999.

[21] Y. Bazilevs, V.M. Calo, T.E. Tezduyar, and T.J.R. Hughes. *YZβ* discontinuity capturing for advection-dominated processes with application to arterial drug delivery. *International Journal for Numerical Methods in Fluids*, 54:593–608, 2007.

[22] Y. Bazilevs, C. Michler, V.M. Calo, and T.J.R. Hughes. Weak Dirichlet boundary conditions for wall-bounded turbulent flows. *Computer Methods in Applied Mechanics and Engineering*, 196:4853–4862, 2007.

[23] Y. Bazilevs, C. Michler, V.M. Calo, and T.J.R. Hughes. Isogeometric variational multiscale modeling of wall-bounded turbulent flows with weakly enforced boundary conditions on unstretched meshes. *Computer Methods in Applied Mechanics and Engineering*, 2008. Published online, doi:10.1016/j.cma.2008.11.020.

[24] T.J.R. Hughes, J.A. Cottrell, and Y. Bazilevs. Isogeometric analysis: CAD, finite elements, NURBS, exact geometry, and mesh refinement. *Computer Methods in Applied Mechanics and Engineering*, 194:4135–4195, 2005.

[25] T.J.R. Hughes, G. Scovazzi, and L.P. Franca. Multiscale and stabilized methods. In E. Stein, R. de Borst, and T. J. R. Hughes, editors, *Encyclopedia of Computational Mechanics, Vol. 3, Computational Fluid Dynamics*, chapter 2. Wiley, 2004.

[26] F. Shakib and T.J.R. Hughes. A new finite element formulation for computational fluid dynamics: IX. Fourier analysis of space-time Galerkin/least-squares algorithms. *Computer Methods in Applied Mechanics and Engineering*, 87:35–58, 1991.

[27] C. Johnson. *Numerical solution of partial differential equations by the finite element method*. Cambridge University Press, Sweden, 1987.

[28] L. Catabriga, A.L.G.A. Coutinho, and T.E. Tezduyar. Compressible flow SUPG stabilization parameters computed from element-edge matrices. *Computational Fluid Dynamics Journal*, 13:450–459, 2004.

[29] L. Catabriga, A.L.G.A. Coutinho, and T.E. Tezduyar. Compressible flow SUPG parameters computed from element matrices. *Communications in Numerical Methods in Engineering*, 21:465–476, 2005.

[30] L. Catabriga, A.L.G.A. Coutinho, and T.E. Tezduyar. Compressible flow SUPG parameters computed from degree-of-freedom submatrices. *Computational Mechanics*, 38:334–343, 2006.

[31] J. Holmen, T.J.R. Hughes, A.A. Oberai, and G.N. Wells. Sensitivity of the scale partition for variational multiscale LES of channel flow. *Physics of Fluids*, 16:824–827, 2004.

[32] T.J.R. Hughes, L. Mazzei, and K.E. Jansen. Large-eddy simulation and the variational multiscale method. *Computing and Visualization in Science*, 3:47–59, 2000.

[33] T.J.R. Hughes, L. Mazzei, A.A. Oberai, and A.A. Wray. The multiscale formulation of large eddy simulation: Decay of homogenous isotropic turbulence. *Physics of Fluids*, 13:505–512, 2001.

[34] T.J.R. Hughes, A.A. Oberai, and L. Mazzei. Large-eddy simulation of turbulent channel flows by the variational multiscale method. *Physics of Fluids*, 13:1784–1799, 2001.

[35] T.J.R. Hughes, G.N. Wells, and A.A. Wray. Energy transfers and spectral eddy viscosity of homogeneous isotropic turbulence: comparison of dynamic Smagorinsky and multiscale models over a range of discretizations. *Physics of Fluids*, 16:4044–4052, 2004.

[36] Y. Bazilevs. *Isogeometric Analysis of Turbulence and Fluid-Structure Interaction*. PhD thesis, ICES, UT Austin, 2006.

[37] P.B. Bochev, M.D. Gunzburger, and J.N. Shadid. On infsup stabilized finite element methods for transient problems. *Computer Methods in Applied Mechanics and Engineering*, 193:1471–1489, 2004.

[38] P.B. Bochev, M.D. Gunzburger, and R.B. Lehoucq. On stabilized finite element methods for the Stokes problem in the small time step limit. *International Journal for Numerical Methods in Fluids*, 53:573–597, 2007.

[39] J.-J. Droux and T.J.R Hughes. A boundary integral modification of the Galerkin least squares formulation for the Stokes problem. *Computer Methods in Applied Mechanics and Engineering*, 113:173–182, 1994.

[40] I. Akkerman, Y. Bazilevs, V.M. Calo, T.J.R. Hughes, and S. Hulshoff. The role of continuity in residual-based variational multiscale modeling of turbulence. *Computational Mechanics*, 41:371–378, 2008.

[41] R. Moser, J. Kim, and R. Mansour. DNS of turbulent channel flow up to $Re = 590$. *Physics of Fluids*, 11:943–945, 1999.